Journal of Hydrology 369 (2009) 175–182

Contents lists available at ScienceDirect

Journal of Hydrology

journal homepage: www.elsevier.com/locate/jhydrol

Physical and isotopic characterization of evaporation from *Sphagnum* moss

Jonathan S. Price [a,*], Thomas W.D. Edwards [b], Yi Yi [b], Peter N. Whittington [a]

[a] Department of Geography and Environmental Management, University of Waterloo, Waterloo, ON N2L 3G1, Canada
[b] Department of Earth and Environmental Sciences, University of Waterloo, Waterloo, ON N2L 3G1, Canada

ARTICLE INFO

Article history:
Received 1 August 2008
Received in revised form 25 January 2009
Accepted 17 February 2009

This manuscript was handled by L. Charlet, Editor-in-Chief, with the assistance of Jiin-Shuh Jean, Associate Editor

Keywords:
Diffusion
Isotopes
Oxygen
Hydrogen
Vapour flow
Capillary flow

SUMMARY

Evaporation from and water transfer within living and dead (but undecomposed) *Sphagnum* mosses is important biologically and hydrologically, but understanding of the internal mass-transfer mechanisms remains incomplete. A column experiment was conducted to characterize liquid and vapour fluxes and the profiles of relative humidity, temperature and the hydrogen- and oxygen-isotope composition of *Sphagnum* pore waters evaporating under controlled conditions. A constant water table at 20 cm depth was established in six identical columns fed by a common water reservoir ($\delta^{18}O = -13.0‰$; $\delta^{2}H = -85.8‰$). Evaporation from the columns averaged 4.5 mm d^{-1} at the average chamber temperature and relative humidity of 20.7 °C and 27.1%, respectively. The columns developed upward-convex profiles of relative humidity and isotopic composition within the first day that persisted throughout the experiment. Isotopic data from columns sampled after 1, 2, 4, 7 and 15 days were strongly constrained by an evaporation line with the linear relation $\delta^{2}H = 3.8\delta^{18}O - 36.1$ ($R^2 = 0.99$; $n = 25$), consistent with the expected evaporative-enrichment trajectory under chamber conditions. Calculated vapour flux accounted for only ~1% of the total mass flux within the columns, reflecting the dominance of liquid-phase capillary flow. While this calculated vapour flux was small, it decreased markedly near the surface, where evaporative cooling may have resulted in condensation of vapour, simultaneously increasing the liquid water content of the surface mosses. The presence of a vapour pressure deficit down to about 15 cm below the surface indicate that both evaporation and upward vapour diffusion were occurring at depth within the *Sphagnum* columns, but modelling shows that in situ fractionation alone within the columns cannot explain the extent of the observed enrichment. Rather, the enrichment of the heavy isotopes wherever evaporation is occurring and their consequent downward diffusion are needed to explain the observed profiles. Coupled advection–diffusion modelling of these profiles yielded estimates of the effective liquid-phase diffusivities in *Sphagnum* pore waters of 2.380 (±0.020) × 10^{-5} cm^2 s^{-1} for $^{1}H^{1}H^{18}O$ and 2.415 (±0.015) × 10^{-5} cm^2 s^{-1} for $^{1}H^{2}H^{16}O$, in good agreement with accepted values.

© 2009 Elsevier B.V. All rights reserved.

Introduction

Water movement in *Sphagnum* mosses is a poorly understood phenomenon, yet it is critically important to peatland evaporation processes (Kellner, 2002), carbon exchanges (McNeil and Waddington, 2003), nutrient translocation (Rydin and Clymo, 1989) and heat flow (Kim and Verma, 1996). Here we refer not to the water exchanges in the peat substrate, for which we have recently gained considerable understanding (e.g. Drexler et al., 1999; Kennedy and Van Geel, 2000; Reeve et al., 2000; Price, 2003; Kellner et al., 2005); rather, we seek to clarify the nature of water fluxes through the matrix of living and dead mosses near the peatland–atmosphere interface.

Mosses comprise a matrix of large pores arising between and within the structure of leaves and branches (Hayward and Clymo, 1982; Clymo and Hayward, 1982) that impart a huge potential range (e.g. ~2–95%) of moisture contents (Boelter, 1970). Saturated water flow can be too fast to measure (e.g. Boelter, 1965), but when the moss is dry the liquid flux is negligible (Ingram, 1983). Upward migration of water above the water table in *Sphagnum* mosses is typically attributed to capillary flow (Hayward and Clymo, 1982). When this flow is inadequate to meet the evaporative demand, the moss begins to dry and the water pressure (ψ) falls quickly. Water can be withdrawn from storage within hyaline cells when ψ drops below −100 kPa and then the moss desiccates (Hayward and Clymo, 1982). At this stage capillary water flow is negligible, but vapour diffusion can still occur. Under these conditions, evaporation cannot proceed efficiently, and several studies have noted a sharp drop in the evaporation rate from mosses as they dry (Price, 1991; Kim and Verma, 1996), suggesting a limited ability to move water up from the water table (see also Kellner and Halldin, 2002). However, field studies report that water lost to evaporation is mostly replaced by upward flow (Yazaki et al., 2006). How does this occur?

* Corresponding author. Tel.: +1 519 888 4567x35711; fax: +1 519 746 0658.
E-mail address: jsprice@envmail.uwaterloo.ca (J.S. Price).

0022-1694/$ - see front matter © 2009 Elsevier B.V. All rights reserved.
doi:10.1016/j.jhydrol.2009.02.044

Typically, evaporation is assumed to occur at the *Sphagnum* surface (e.g. Nichols and Brown, 1980), which would require delivery of water by capillary action to the sites where turbulent and radiant exchanges occur. However, latent heat exchanges can also occur below the soil surface (Cahill and Parlange, 1998), indicating that water moves in both liquid and vapour phases. The vapour flux increases where there are large pores and strong thermal and moisture gradients (Yoshikawa et al., 2002; Williams and Flanagan, 1996), especially when there is a strong surface wind (Ishihara et al., 1992). In dry soils the vapour flux can be comparable to the liquid flux (Rose, 1968) and is typically attributed to diffusion, but occurs by advection caused by temperature and pressure changes in some cases, and by wind pumping (Stern et al., 1999) and water infiltration (Touma et al., 1984). In forest mosses, Carleton and Dunham (2003) showed that vapour diffusion accompanied by diurnal cooling of the upper moss layers caused "distillation" or condensation of vapour in the upper layers. While physiologically important, this yields a relatively small quantity of water.

Insight into the evaporation process and water flux in the soil can be gained by observing the nature and extent of isotopic fractionation and redistribution in a soil profile. Evaporation from peatlands causes enrichment of ^{18}O and ^{2}H in the near-surface pore waters (Williams and Flanagan, 1996; Flanagan et al., 1997) and signals from this evaporative enrichment are subsequently incorporated into associated plant tissues (Brenninkmeijer et al., 1982; Edwards, 1993). Aravena and Warner (1992) showed that differences in evaporation rates between adjacent hummocks and hollows could be detected in the ^{18}O content of *Sphagnum* cellulose, suggesting that pore-water isotopic composition may be a sensitive monitor of water dynamics within peatlands.

Exponentially-declining ^{18}O and ^{2}H abundances occur in saturated and unsaturated soil columns undergoing evaporation (Zimmermann et al., 1967; Münnich et al., 1980; Allison et al., 1983; Allison and Barnes, 1983; Barnes and Allison, 1983, 1988; Walker et al., 1988; Barnes and Walker, 1989; Hsieh et al., 1998; DePaolo et al., 2004). These upward-convex profiles reflect competition between the downward diffusion of $^{1}H^{1}H^{18}O$ and $^{1}H^{2}H^{16}O$ molecules concentrated at the surface and the upward flow of liquid water that sustains the evaporation flux. The profiles can be modelled to estimate evaporation rates under steady and non-steady conditions, assuming knowledge of the liquid-phase diffusivities of the respective isotope species. As highlighted by Barnes and Allison (1988), however, vapour-phase diffusion and vapour–liquid exchange also play key roles in the evaporation process in unsaturated soils by "short-circuiting" across air-filled pores, thus transmitting isotopic signals downward more quickly than liquid-phase diffusion alone would allow in a saturated soil.

Here we report results from similar experiments designed to improve our understanding of water transport in *Sphagnum* moss undergoing evaporation. Specifically, our analysis included (1) quantitative partitioning of the net liquid and vapour fluxes, confirming the overwhelming importance of liquid-phase mass transfer by capillary flow, and (2) advection–diffusion modelling to probe the nature of the pore-water isotopic profiles that were obtained. The latter sheds new light on the fundamental influence that vapour diffusion and vapour–liquid exchange have on hydrologic and isotopic processes in the unsaturated zone of *Sphagnum*-dominated peatlands.

Methods

Experimental procedure

Our approach was to allow evaporation from columns of relatively undisturbed *Sphagnum rubellum* moss samples having a constant water table supplied with water from a common isotopic source. During the experiment, we determined depth profiles of water content, relative humidity of pore gas, isotopic composition of pore water and soil properties. A large (45 × 45 × 25 cm) block of hummock peat was extracted from a southern Ontario bog (43° 90′ N, 80° 40′ W) in December 2005. The hummock was frozen during removal and thus compression and disturbance during cutting were minimal. In the laboratory, the frozen sample was subdivided and trimmed to fit snugly into six 15 cm diameter × 25 cm long PVC cylinders; vascular vegetation protruding from the samples was clipped. PVC end caps fitted to the bottom end of each core were connected by a screened flexible manometer hose to a common reservoir. The samples were twice completely filled with deionised water from a reservoir and allowed to drain for 24 hours before commencing the experiment. Tests conducted with waters of two different isotopic compositions using a *Sphagnum* column from the same block of hummock peat confirmed that this double-flushing procedure effectively re-sets the $\delta^{18}O$ and $\delta^{2}H$ of *Sphagnum* pore waters to that of the reservoir water.

The six manometer tubes and common water supply reservoir were positioned to hold the water table 5 cm above the base of each core (20 cm below the surface) and a secondary reservoir maintained a constant head in the primary reservoir (Fig. 1). The secondary reservoir was covered to prevent any changes in isotopic signature due to evaporation but had a small vent to maintain atmospheric pressure. The apparatus was set-up in a darkened chamber (~3 × 4 × 4 m), with a grow light set to a 12-h cycle. A fan in the chamber directed air away from the samples to maintain air circulation, and a Hobo U10 relative humidity sensor simultaneously logged chamber air temperature (*T*) and relative humidity (*RH*).

One of the six samples in the chamber had thermocouples embedded at the surface (0–1 cm), 5, 10, 15, 20, and 25 cm, respectively, connected to a Campbell Scientific 10x logger to record moss temperature (T_0, T_5, etc.) every 30 min. Temperature at 2.5 cm depth was linearly interpolated from the 0–1 and 5 cm thermocouples. This and the remaining columns were left to allow evaporation for 1, 2, 4, 7 and 15 days, respectively. At the designated time, each column was disconnected from the water supply, but

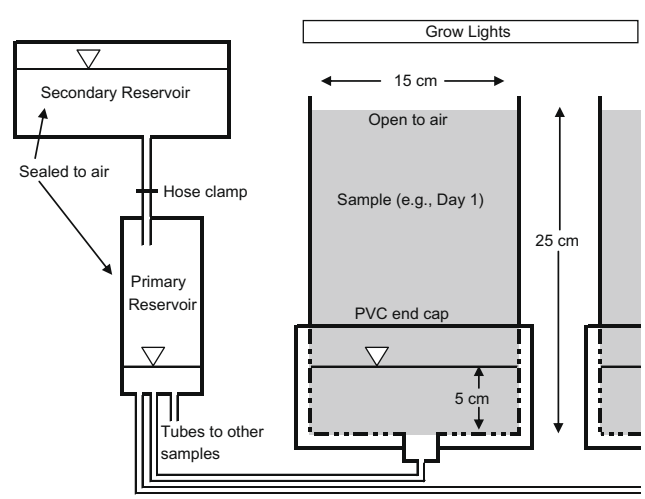

Fig. 1. Schematic of laboratory instrumentation. The primary and secondary reservoirs were sealed to the air and connected with a tube clamped to control flow. The primary reservoir was smaller and narrower than the secondary so that a more accurate water table could be maintained. The reservoir was coupled to separate columns that were sectioned after 1, 2, 4, 7 and 15 days, plus an additional column that was instrumented with thermocouples at 0 to 1, 5, 10, 15, 20, and 25 cm. *RH* was measured at 2.5 cm depth increments to 15 cm depth on the day the respective column was sectioned.

prior to disconnection *RH* was measured at 2.5 cm depth increments to 15 cm depth with a Vaisala relative humidity micro probe (HMP42). At the ambient humidity levels (93–100%) its reported accuracy and precision are 3% and 0.1%, respectively. Immediately after removal, the sample was sectioned as follows. The PVC column was gently removed by sliding it upwards out of the end-cap and over the core, leaving the *Sphagnum* core standing undisturbed in the end-cap with the water table maintained 5 cm above the base. First, a 5-cm section was cut from the top of the core and placed immediately into a plastic bag and sealed after removing most of the air, followed sequentially by the four remaining sections. This process was accomplished in less than 5 min so that evaporation from the sides of the sample (briefly exposed to the air) was negligible. The sample was then squeezed inside the plastic bag until water pooled – the elution being decanted into a 30 ml sample bottle and sealed. Two additional samples were taken from the secondary water supply reservoir on Day 1 and Day 15 to confirm that no changes had occurred in the source water isotopic composition.

The sixth column (instrumented with thermocouples) was similarly sectioned to evaluate the volumetric moisture content, porosity, particle density and bulk density using standard methods (Klute, 1986). The evaporation rate from this and the other columns was determined by the rate of water loss from the secondary reservoir, based on the appropriate time and number of columns left in the series. This assumes that the evaporation rate was identical for all columns at any given time, although fluctuations in chamber humidity (and thus evaporation rate) did occur during the course of the experiment.

Isotopic analysis

Water samples were analyzed in the Environmental Isotope Laboratory at the University of Waterloo, where $^{18}O/^{16}O$ and $^{2}H/^{1}H$ ratios were measured using standard methods (Epstein and Mayeda, 1953; Coleman et al., 1982; see Drimmie and Heemskerk, 1993). Results are reported in δ values, representing deviations in per mil (‰) from Vienna-Standard Mean Ocean Water (V-SMOW) on a scale normalized such that Standard Light Antarctic Precipitation (SLAP) has values of −55.5‰ ($\delta^{18}O$) and −428‰ ($\delta^{2}H$) as recommended by Coplen (1996). $\delta^{18}O$ or $\delta^{2}H = 1000\ [(R_{sample}/R_{V\text{-}SMOW}) - 1]$, where R is the ratio of $^{18}O/^{16}O$ or $^{2}H/^{1}H$ in the sample and V-SMOW, respectively. Analytical uncertainties are ±0.2‰ for $\delta^{18}O$ and ±2.0‰ for $\delta^{2}H$.

Partitioning of vapour and liquid mass fluxes

The bulk upward flux of water is a combination of vapour diffusion and liquid advection. Vapour diffusion flux (F_v) in the columns can be calculated according to Fick's first law (Millington, 1959) accounting for the effects of soil porosity (φ) and air-filled porosity (ε) (Millington and Quirk, 1961, cited in Moldrup et al., 2000) such that

$$F_v = D_v^* \left(\frac{\varepsilon^{10/3}}{\phi^2}\right) \frac{\partial C_v}{\partial z} \tag{1}$$

where D_v^* is the diffusion coefficient of water vapour in air, C_v is the concentration of water vapour and z is the depth ordinate. Air-filled porosity is determined as

$$\varepsilon = 1 - \theta - \frac{\rho_b}{\rho_p} \tag{2}$$

where θ is volumetric moisture content, ρ_b is bulk density and ρ_p is particle density. D_v^* may be calculated as (Gates, 1980)

$$D_v^* = 0.212(1 + 0.0071T)\,\mathrm{cm^2 s^{-1}} \tag{3}$$

where T is temperature (°C). Vapour concentration (C_v) can be determined from the ideal gas law using the partial pressure of moisture (e), calculated from measurements of relative humidity (RH), temperature (T) and saturation vapour pressure (e_{sat}), where

$$RH = \frac{e}{e_{sat}} \tag{4}$$

and

$$e_{sat} = 610.78^{\left(\frac{T}{T+238.3}17.269\right)}\ \mathrm{kPa} \tag{5}$$

(Tetens, 1930; see Govardhan and Alex, 2005), so that $C_v = 0.002166\ e/(T + 273.15)\ \mathrm{kg/m^3}$.

Modelling of the isotopic profiles

We used advection–diffusion modelling to analyze the observed isotopic profiles, following a similar approach to that of Barnes and Allison (1983, 1988) and Allison et al. (1983), though modified to allow for mass-dependent differences in the liquid-phase diffusivities of the different water-isotope species (*cf.* Mathieu and Bariac, 1996; DePaolo et al., 2004).

According to Darcy's Law:

$$\frac{F_l}{\rho} = -K\frac{dh}{dz} \tag{6}$$

where F_l is the flux in the liquid phase (g cm^{-2} s^{-1}), ρ is the density of liquid water (g cm^{-3}), K is the hydraulic conductivity of the *Sphagnum* column (cm s^{-1}), h is the water head (cm), and z is the depth (cm). Water is evaporatively enriched in the heavy-isotope species ($^{1}H^{1}H^{18}O$ and $^{1}H^{2}H^{16}O$) at the top of the columns and relatively depleted in these species at the bottom. Under conditions of hydrologic and isotopic steady-state, the net fluxes in heavy-isotope species, which are the respective differences between upward advective flux and downward diffusive fluxes, will also reach a constant value at any given depth within the profile.

The flux of heavy-isotope species therefore can be expressed by the equation:

$$F_l^i = F_l \cdot R_L + \left(-D_l^{*i} \cdot \frac{dC_l^i}{dz}\right) \tag{7}$$

where the superscript i indicates water molecules containing the respective heavy isotopes, R_L is the isotopic ratio of liquid water ($R_L = {}^{18}O/^{16}O$ or $^{2}H/^{1}H$), D_l^* is the effective liquid-phase diffusivity (cm^2 s^{-1}), with D_l^{*i} signifying water molecules containing heavy isotopes, and C_l^i (g cm^{-3}) is the concentration of heavy water molecules in the liquid phase.

By definition, C_l^i is the mass divided by volume, therefore:

$$C_l^i = \frac{M^i}{V} = \frac{M^i}{M}\cdot\frac{M}{V} = \frac{N^i m^i}{Nm}\cdot\rho = \frac{m^i}{m}R_L\rho \tag{8}$$

where M (g) is the mass of water, V (cm^3) is the volume of the water, m (g mol^{-1}) is the molecular weight of water molecules, N (mol) represents the number of water molecules, and ρ (g cm^{-3}) is the density of the water.

Substituting (8) into (7), and treating ρ as constant because of the small range of temperature, yields the expression:

$$F_l^i = F_l \cdot R_L - D_l^{*i}\frac{m^i}{m}\rho\cdot\frac{dR_L}{dz} \tag{9}$$

which describes the relationship among isotopic fluxes in the liquid phase (F_l^i and F_l), the isotope ratio of water (R_L) and depth (z).

The respective steady-state fluxes can be described by $F_l + F_v = Inflow$ and $F_l^i + F_v^i = Inflow^i$, which can be combined to give:

$$\frac{F_l^i + F_v^i}{F_l + F_v} = R_{Input} \tag{10}$$

which is consistent with steady-state quantitative conversion of water from the liquid to vapour phase (i.e., without isotopic fractionation).

This can be simplified to a good first-order approximation knowing $F_l \gg F_v$ and $F_l^i \gg F_v^i$ (calculated above), such that:

$$R_{Input} = \frac{F_l^i}{F_l} \tag{11}$$

Rearranging Eq. (11) and substituting in Eq. (9) then yields:

$$F_l \cdot R_{input} = F_l \cdot R_L - D_l^{*i} \cdot \frac{m^i}{m} \rho \cdot \frac{dR_L}{dz} \tag{12}$$

Rearrangement of (12) gives

$$\frac{dR_L}{R_L - R_{input}} = \frac{mF_l}{m^i \cdot D_l^{*i} \cdot \rho} \cdot dz \tag{13}$$

which expresses the isotopic ratio of water (R_L) as a function of depth. Integrating (13) from the surface ($z = 0$) to depth z yields:

$$\int_{R_{surface}}^{R_L} \frac{dR_L}{R_L - R_{input}} = \int_0^z \frac{mF_l}{m^i \cdot D_l^{*i} \cdot \rho} \cdot dz \tag{14}$$

Since R_{input}, ρ and D_l^{*i} are constant, the results of integration can be expressed as:

$$\ln\left(\frac{R_L - R_{Input}}{R_{Surface} - R_{Input}}\right) = \frac{mF_l}{m^i \cdot D_l^{*i} \cdot \rho} \cdot z \tag{15}$$

Converting Eq. (15) into δ notation gives:

$$\ln\left(\frac{\delta_L - \delta_{Input}}{\delta_{Surface} - \delta_{Input}}\right) = \frac{mF_l}{m^i \cdot D_l^{*i} \cdot \rho} \cdot z \tag{16}$$

which expresses the relation between the isotopic composition of pore water (δ_L) and the sampling depth (z). Plotting $\frac{\delta_L - \delta_{Input}}{\delta_{Surface} - \delta_{Input}}$ against z yields an exponential profile, thus affording the opportunity to test whether the measured *Sphagnum* pore-water isotopic profiles obtained from the column experiment reflect steady-state conditions and, if so, to determine the effective liquid-phase diffusivities for $^1H^1H^{18}O$ and $^1H^2H^{16}O$ in this porous medium.

The evaporative-enrichment response of the *Sphagnum* pore waters can be assessed by considering the special case of the Craig and Gordon (1965) model describing the isotopic composition of a terminal reservoir evaporating in isotopic and hydrologic steady-state:

$$\delta_{Water} = \alpha_e \alpha_k (1 - RH)(\delta_{Input} + 1000) + \alpha_e RH(\delta_{Air} + 1000) - 1000 \tag{17}$$

where α_e represents the respective temperature-dependent liquid–vapour equilibrium fractionation factors of 1.0097 and 1.0835 for ^{18}O and ^2H at mean experimental temperature of 20.7 °C (calculated from equations reported by Horita and Wesolowski, 1994); α_k represents the respective kinetic fractionations of 1.0142 and 1.0125 for open-water evaporation (see Gonfiantini, 1986); *RH* represents mean relative humidity in decimal notation (0.271); δ_{Input} represents the respective $\delta^{18}O$ and δ^2H values of input water (−13.0‰ and −85.8‰) and δ_{Air} represents the respective $\delta^{18}O$ and δ^2H values of ambient atmospheric moisture (−20.5‰ and −149.1‰; based on isotopic equilibrium with local tap water used to humidify the laboratory ventilation system).

The slope of the evaporation line (S_{EL}) is then given by:

$$S_{EL} = (\delta^2H_{Water} - \delta^2H_{Input})/(\delta^{18}O_{Water} - \delta^{18}O_{Input}). \tag{18}$$

Results

Bulk density (ρ_b) increased with depth, but in the unsaturated zone (0–20 cm) was fairly constant at 0.15–0.20 g cm^{-3} (Table 1). Porosity (φ) decreased with depth. The moisture content ranged from 14.1% near the surface to 25.9% near the base of the unsaturated zone.

Chamber temperature (T) was relatively stable during the experiment (average ± standard deviation = 20.7 ± 0.6 °C) (Tables 2 and 3). Instrument failure meant no *RH* data were available until partway through Day 2 (see Table 2). Variably high *RH* subsequently occurred during the Day 3–10 period (average 31.3%) because of servicing of the laboratory ventilation system, before stabilizing over the Day 11–15 period (average 23.0%). The average evaporation loss from the columns over the span of the experiment was 4.5 mm d^{-1}. Weighting to account for variations in chamber *RH* yielded estimated average daily evaporation ranging from 3.9 mm d^{-1} (Day 7) to 4.8 mm d^{-1} (Day 15).

The columns were distinctly cooler at the surface (Fig. 2a), and the temperature gradient above the water table was similar in each column. The temperature profile was distinctly lower on Day 15 (Fig. 2) reflecting the coolest daily average temperature (19.0 °C) in the chamber, compared to the average of 20.7 °C (Table 2). On Day 7 the temperature in the profile was highest, reflecting relatively warm conditions in the chamber, and resulted in the highest profile *RH* (Fig. 2). Relative humidity was lowest near the surface (Fig. 2b), thus vapour concentration (C_v) decreased upward (Fig. 3a). The vapour concentration gradient ($\delta C_v/\delta z$) was similar in each column. Calculated upward vapour flux in the columns (Eq. (1)) averaged less than 0.04 mm d^{-1} (Fig. 3b).

Relative to the $\delta^{18}O$ and δ^2H values of source water (average −13.0‰ and −85.8‰, respectively) enrichment was greatest near

Table 1
Physical properties of *Sphagnum*, including dry bulk density and volumetric moisture content (VMC).

Depth (cm)	Bulk density (g/cm^3)	VMC
0–5	0.018	14.1
5–10	0.017	13.0
10–15	0.015	13.7
15–20	0.020	25.9
20–25	0.037	77.4

Average particle density (ρ_p) 1.2 g cm^{-3}.

Table 2
Daily average chamber air temperature (T) and relative humidity (*RH*) measured with the Hobo U10, and the evaporation rate (E) from the *Sphagnum* columns estimated from the rate of water loss from the reservoir.

Day	T (°C)	*RH* (%)	E (mm d^{-1})
1	20.8	–	–
2	21.0	–	–
3	20.9	28.4	4.4
4	21.1	32.8	4.1
5	21.1	31.4	4.2
6	21.1	33.7	4.1
7	21.1	36.6	3.9
8	21.4	33.0	4.1
9	21.1	27.9	4.4
10	20.9	26.3	4.5
11	20.8	24.1	4.7
12	20.5	22.9	4.7
13	20.2	23.5	4.7
14	19.8	23.2	4.7
15	19.0	21.4	4.8
Average	20.7	28.1	4.5
St.Dev	0.6	5.1	–

Table 3
Daily values of ^{18}O and ^{2}H in the supply reservoir (Day 0 and Day 15) and in the monoliths at five depths.

Sample		^{18}O (‰)	Repeat	^{2}H (‰)	Repeat
DAY 0	Supply	−12.81		−85.41	−85.67
DAY 1	0–5	−6.58	−6.87	−60.07	−59.51
DAY 1	5–10	−11.23		−80.04	−79.36
DAY 1	10–15	−11.87		−81.42	−81.48
DAY 1	15–20	−12.15		−83.52	−84.06
DAY 1	20–25	−12.51		−84.19	−84.34
DAY 2	0–5	−7.66	−7.62	−64.22	−64.37
DAY 2	5–10	−11.02		−76.51	−76.48
DAY 2	10–15	−12.22		−82.24	−82.19
DAY 2	15–20	−12.72	−12.59	−84.20	−84.13
DAY 2	20–25	−12.80		−84.13	−84.50
DAY 4	0–5	−4.89		−55.10	−56.26
DAY 4	5–10	−11.15	−11.51	−76.87	−77.11
DAY 4	10–15	−12.44		−82.46	−82.71
DAY 4	15–20	−12.53		−84.63	−84.36
DAY 4	20–25	−12.96		−83.87	−84.02
DAY 7	0–5	−6.03		−61.25	−59.99
DAY 7	5–10	−11.92		−80.73	−81.80
DAY 7	10–15	−12.66	−12.73	−84.00	−83.89
DAY 7	15–20	−12.87		−84.25	−84.76
DAY 7	20–25	−12.91		−85.06	−85.51
Day 15	0–5	−7.67		−64.84	−64.53
Day 15	5–10	−11.11		−78.77	−77.49
Day 15	10–15	−12.37		−84.14	−85.69
Day 15	15–20	−13.07	−12.86	−85.31	−86.07
Day 15	20–25	−13.09		−85.55	−85.83
Day 15	Supply	−13.13		−86.68	−85.36

the surface (average −6.6‰ and −61.0‰, respectively) (Fig. 4a and b). The enrichment decreased exponentially with depth, converging on the isotopic composition of the reservoir at the base of each column (20–25 cm interval). The profiles exhibited small systematic variations between successive sample days, although nearly identical profiles within analytical uncertainties were obtained on Days 2 and 15. The isotopic data from all columns cluster tightly along a line in $\delta^{18}O$-$\delta^{2}H$ space (Fig. 4c) described by:

$$\delta^2H = 3.8\delta^{18}O - 36.1 \quad (r^2 = 0.99) \tag{19}$$

which exactly matches the expected trajectory of evaporative enrichment for surface waters evaporating under our experimental conditions using Eqs. (17) and (18).

Discussion

Physical processes

Evaporation from the samples caused cooling, and consequently temperature gradients developed in each column. Variations in air temperature in the chamber were not large (Table 2). Nevertheless, they caused a shift in the absolute temperature of the samples, although the temperature gradients remained similar on most days (Fig. 2a). Evaporation was occurring not just from the moss surface, but the presence of a vapour pressure deficit (*RH* < 100%), especially in the top 5 cm (Fig. 2b), suggests that latent heat exchanges were occurring at depth. That the pore atmosphere remained below vapour saturation (Fig. 2b) implies either a water vapour flux (loss), or condensation elsewhere within the sample. Collis-George (1959) noted that *RH* in soil pores is reduced to 98.5% when the tension is at the wilting point (−15,000 cm of water), or where there are highly negative solute potentials (Izbicki et al., 2000), because of condensation effects. Neither of these (very low potentials) was present in this case.

The presence of temperature and vapour concentration gradients indicate that both heat and vapour flowed towards the surface, although the very small calculated vapour diffusive flux

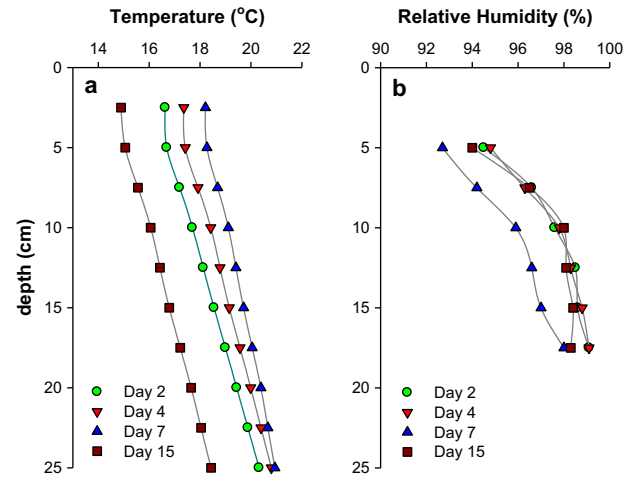

Fig. 2. Profiles of average daily *T* (a) measured in the instrumented column and *RH* (b) on Days 2, 4, 7 and 15 measured in the respective columns prior to sectioning.

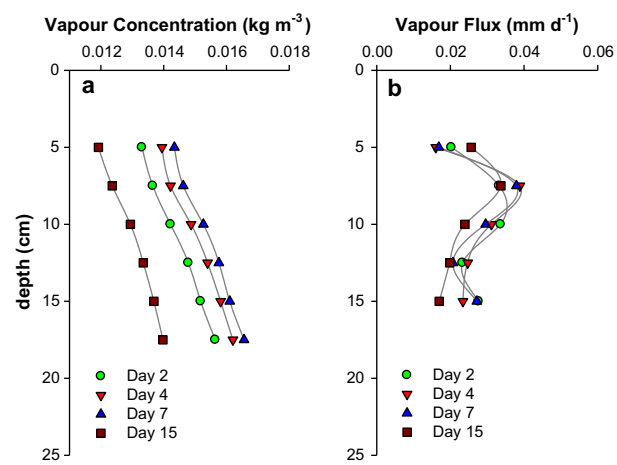

Fig. 3. Profiles of measured vapour concentration (a) and calculated diffusive vapour flux (b) on Days 2, 4, 7 and 15.

(0.04 mm d^{-1}) represented ~ 1% of the evaporative water loss from the columns. The abrupt decrease in the calculated flux near the surface (Fig. 3b) is an artefact of the inflection point (i.e. slight decrease) of the temperature gradient above 5 cm depth (Fig. 2a), since *RH* is related to temperature. Advective vapour exchange can also occur due to the expansion and contraction of gas with temperature change and by atmospheric pressure changes (Stern et al., 1999). Based on the ideal gas law, changes in gas volume can be determined for given changes in temperature and pressure. In the chamber the diurnal temperature changes (±2 °C) caused less than 1% gas volume change. Over the duration of the experiment the range of atmospheric pressure changes of 3.66 kPa (University of Waterloo, 2006) would result in ~5% gas volume change (daily pressure changes averaged <1 kPa). Thus we believe that temperature and pressure changes had a negligible effect on vapour exchanges, and conclude that vapour diffusion is more important than advective vapour flow. While this vapour flux is small, it may be important in maintaining sufficiently moist conditions for biological productivity (Carleton and Dunham, 2003).

Isotopic processes

The presence of a vapour pressure deficit in the *Sphagnum* columns indicates potential for in situ fractionation. However,

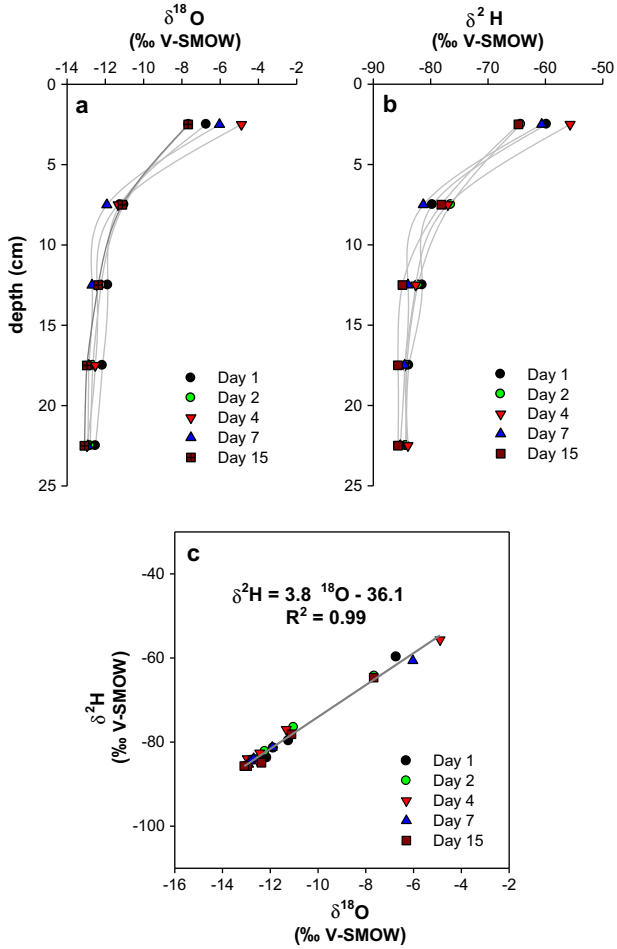

Fig. 4. δ^{18}O (a) and δ^{2}H (b) for pore waters in the *Sphagnum* columns, and the relationship between the two (c), revealing the upward-convex profiles and the tight clustering around a common evaporation line.

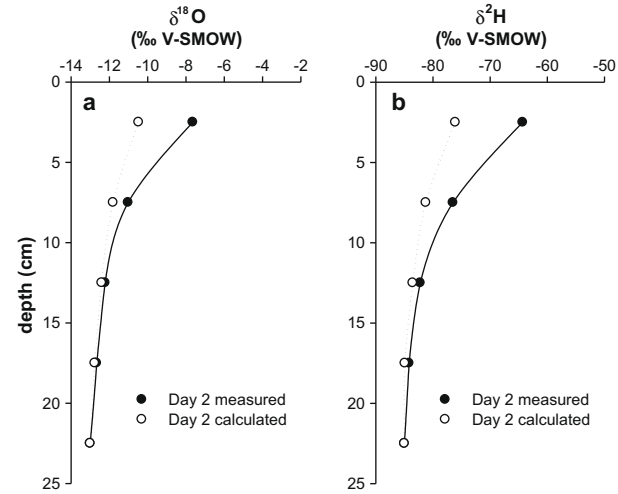

Fig. 5. Measured and calculated profiles of δ^{18}O (a) and δ^{2}H (b) for Day 2. The calculated profiles are based on steady-state evaporative isotopic enrichment for each segment at measured *T* and *RH*, as described by Eq. (17), with input water and associated ambient vapour supplied by the underlying segment. This reproduces the observed evaporation line slope of 3.8, but does not generate the observed overall extent of enrichment for either heavy isotope.

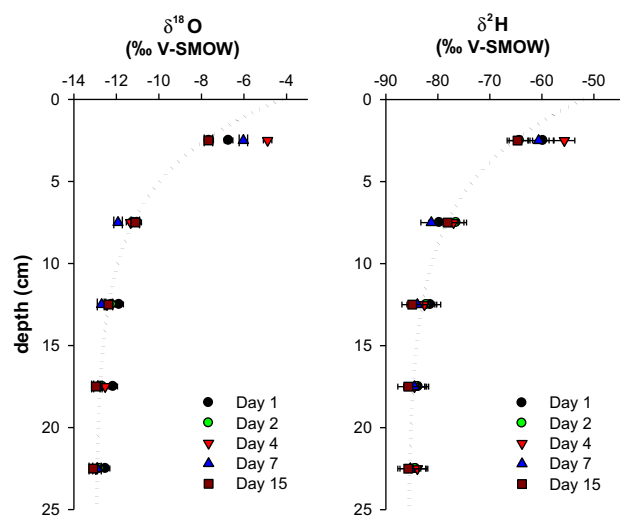

Fig. 6. Comparison of measured isotopic data for Days 2, 4, 7 and 15 with simulated steady-state isotopic profiles generated using a coupled advection-diffusion model. The dotted lines are constrained to the observed evaporation line (Fig. 4c) and fitted to the isotopic data for Days 2 and 15, as explained in the text. The error bars reflect analytical uncertainties of ±0.2‰ for δ^{18}O and ±2.0‰ for δ^{2}H.

calculated steady-state evaporative enrichment using the Craig and Gordon (1965) model alone cannot fully account for the observed profiles (Fig. 5). Rather, downward heavy-isotope diffusion is required to magnify the signal.

Simulation of the pore-water isotopic profiles on different sampling days was undertaken assuming that the upward advective flux was 99% of the estimated net evaporation rate, and that pore water δ^{18}O and δ^{2}H values were constrained to the observed evaporation line (Eq. (18)). Pairs of exponential curves generated using Eq. (16) were then compared to the observed profiles, adjusting the respective $\delta_{Surface}$ values and effective liquid-phase diffusion coefficients to explore possible matches. This approach differs somewhat from that taken by Barnes and Allison (1983) and many subsequent authors by not assuming the same liquid-phase diffusion coefficients for the two heavy-isotope species, although the respective values are expected to be very similar.

As shown in Fig. 6, an exact overall match for pairs of profiles simulated in this manner could only be obtained for the measured data from Days 2 and 15, whereas pairs of exponential profiles could not be fitted to data from Days 1, 4 or 7 within analytical uncertainties. The resulting pair of best-fit profiles for Days 2 and 15 yielded $\delta^{18}O_{Surface}$ and $\delta^{2}H_{Surface}$ values of −4.2‰ and −52.0‰ and D_l^{*i} estimates of 2.3 (±0.1) × 10^{-5} cm^2 s^{-1} for $^1H^1H^{18}O$ and 2.6 (±0.2) × 10^{-5} cm^2 s^{-1} for $^1H^2H^{16}O$. These D_l^{*i} estimates agree well with values in the range 2.2–2.7 × 10^{-5} cm^2 s^{-1} that are commonly assumed for $^1H^1H^{18}O$ and $^1H^2H^{16}O$ in studies of soil and leaf waters (e.g., Barnes and Allison, 1988; Mathieu and Bariac, 1996; Gan et al., 2003; DePaolo et al., 2004; Farquhar and Cernusak, 2005; Ogée et al., 2007; etc.). As often noted, however, such values are typically higher than would be expected for reported experimental temperatures. Our estimates, for example, correspond to a "best-fit" temperature of 27.6 ± 0.4 °C according to the temperature-dependent relations presented in Braud et al. (2005), versus temperatures of 16–20 °C measured in the *Sphagnum* columns. Notably, this also places slightly tighter constraints on our estimates of the respective D_l^{*i} values in order to maintain the expected mass-dependent D_l^{*18}/D_l^{*2} ratio of 0.9833 (Mathieu and Bariac, 1996; DePaolo et al., 2004), yielding 2.380 (±0.020) × 10^{-5} cm^2 s^{-1} for $^1H^1H^{18}O$ and 2.415 (±0.015) × 10^{-5} cm^2 s^{-1} for $^1H^2H^{16}O$ under the conditions of our experiment.

The exact agreement between simulated and measured isotopic profiles on Days 2 and 15 strongly suggest that the *Sphagnum* col-

umns were in isotopic steady-state on these days. There is little doubt that this is the case on Day 15, which had the most stable antecedent conditions, especially with respect to *RH* (Table 2). Even a fully saturated soil column (i.e., absent the effects of vapour diffusion and exchange) would be expected to attain steady-state for both isotopes under these experimental conditions after about ten days, as estimated from the effective liquid-phase diffusivities and evaporation rate (E), based on the equation:

$$\tau = D_l^{*i}/E^2 \tag{20}$$

where τ is the characteristic time for profile development (Zimmermann et al., 1967; Allison and Barnes, 1983). Interestingly, the prior occurrence of identical profiles on Day 2 suggests that steady-state had already been attained, at least briefly, for both isotopes prior to the period of higher and variable chamber *RH* during Days 3–10. While we have incomplete documentation of antecedent *RH* for Day 2, its similarity to that of Day 15 suggests *RH* was similar to that of the Day 11–15 interval. The rapid development of isotopic steady-state is thus consistent with the expected importance of vapour–liquid exchange and vapour diffusion within the air-filled porosity of the *Sphagnum* moss, promoted by the four orders-of-magnitude higher vapour-phase diffusivities of the heavy-isotope species (similar to that of bulk water, see Eq. (3) above). That is, liquid-phase diffusion alone cannot explain the rapid establishment of the observed isotopic profiles; the relatively high vapour-phase diffusivities and vapour–liquid exchange thus accelerate their development. These processes also mask the effects of liquid-phase tortuosity in the unsaturated zone by short-circuiting the more tortuous liquid flow paths.

The simulated profiles additionally provide convenient reference lines for assessing the transient behaviour of the profiles on other days. For example, the higher δ^{18}O and δ^2H values in the 0–5 cm layer on Days 4 and 7 likely reflect "excess" downward diffusion of heavy-isotope species from the surface because of decreased evaporation (and hence advection) rate in response to higher *RH*, while the slightly lower δ^{18}O and δ^2H values in the underlying 5–10 cm layer (most clearly apparent on Day 7) reflect associated capillary rise, drawing up isotopically-depleted pore waters from below. Because of incomplete chamber *RH* data, the similarly-distorted profile on Day 1 is more equivocal, yet it also clearly indicates the existence of non-steady-state for both isotopes only one day (and perhaps much less) prior to sampling on Day 2. This suggests that the behaviour of the *Sphagnum* moss pore waters is remarkably analogous to that of water in transpiring leaves, which develop isotopic steady-state within hours (e.g., see Gan et al., 2003; Cuntz et al., 2007; Ogée et al., 2007). Indeed, water mass and isotope transport in the *Sphagnum* columns appears to bear striking similarity to new conceptualizations of how water is transported within transpiring leaves, although the understanding of vapour-phase processes remains incomplete (Cuntz et al., 2007).

Conclusions and implications

These results confirm that water flux in *Sphagnum* moss undergoing evaporation is predominantly liquid capillary flow. In spite of the large air-filled pore spaces, water vapour transport by diffusion represents a negligible fraction of the net mass flow. On the other hand, vapour-phase processes foster rapid development of isotopic steady-state. The dynamic balance between liquid-phase advection and diffusion determines the shapes of the isotopic profiles, while vapour diffusion and vapour–liquid exchange control the rate at which the profiles form and how rapidly they adjust to changing conditions, especially shifts in atmospheric relative humidity. Changes in relative humidity strongly affect upward advection, via changes in evaporation rate, as well as the enrichment of heavy-isotope species near the *Sphagnum* surface, which determines the isotopic concentration gradients within underlying layers. In spite of the rudimentary nature of our experimental set-up, we obtained remarkably robust estimates of the effective liquid-phase diffusivities of $^1H^1H^{18}O$ and $^1H^2H^{16}O$ for *Sphagnum* pore waters, suggesting that potential also exists for application of water-isotope tracers in field-based studies to probe hydrologic processes in *Sphagnum*-dominated wetlands.

These findings have several other important implications. First, they suggest that water flux in mosses can be modelled considering only liquid flow, given the appropriate parameter and boundary conditions. Second, while the change of state from liquid to gas may generate little water volume for vapour flow, it likely results in latent heat exchanges in the profile and thus affects the thermodynamics of the moss system. This has implications for carbon exchange, which is closely tied to moisture and temperature (McNeil and Waddington, 2003). Finally, it is noteworthy that latent heat exchanges caused by evaporation below the soil surface will also affect the determination of soil heat flux, thus potentially causing error in determining available energy for evaporation. Models of evapotranspiration such as the Penman-Monteith (Monteith, 1965) assume that the radiative and convective fluxes occur at a common surface, which may therefore limit their validity in moss-dominated systems.

In *Sphagnum*-dominated systems, translocation of water and presumably other chemical species occur predominantly as liquid capillary flow, but vapour movement also has several implications: (1) upwardly flowing vapour may condense near the evaporatively cooled surface, providing a quantitatively small but potentially important water source for dry surface mosses; and (2) vapour-phase processes accelerate the development of steady-state isotope profiles. Furthermore, the shape of steady-state pore-water isotopic profiles obtained from mosses subjected to evaporation may be useful in estimating evaporation rates in field studies. Samples taken simultaneously from different moss species or in a different setting within a given bog that exhibit distinctly different isotopic profiles may be indicative of differing evaporation rates. Further testing of this possibility in field and laboratory studies is certainly warranted.

Acknowledgement

The financial support of the Natural Sciences and Engineering Research Council (NSERC) of Canada is gratefully acknowledged.

References

Allison, G.B., Barnes, C.J., 1983. Estimation of evaporation from non-vegetated surfaces using natural deuterium. Nature 301, 143–145.
Allison, G.B., Barnes, C.J., Hughes, M.W., 1983. The distribution of deuterium and ^{18}O in dry soils 2: experimental. Journal of Hydrology 64, 377–397.
Aravena, R., Warner, B.G., 1992. Oxygen-18 composition of *Sphagnum*, and microenvironmental water relations. Bryologist 95, 445–448.
Barnes, C.J., Allison, G.B., 1983. The distribution of deuterium and ^{18}O in dry soils 1. Theory. Journal of Hydrology 60, 141–156.
Barnes, C.J., Allison, G.B., 1988. Tracing of water movement in the unsaturated zone using stable isotopes of hydrogen and oxygen. Journal of Hydrology 100, 143–176.
Barnes, C.J., Walker, G.B., 1989. The distribution of deuterium and oxygen-18 during unsteady evaporation. Journal of Hydrology 112, 55–67.
Boelter, D.H., 1965. Hydraulic conductivity of peats. Soil Science 100, 227–231.
Boelter, D.H., 1970. Water table drawdown around an open ditch in organic soils. Journal of Hydrology 15, 329–340.
Braud, I., Bariac, T., Gaudet, J.P., Vauclin, M., 2005. SiSPAT-Isotope a coupled heat water and stable isotope (HDO and $H_2{}^{18}O$) transport model for bare soil Part I Model description and first verifications. Journal of Hydrology 309, 277–300.
Brenninkmeijer, C.A.M., van Geel, B., Mook, W.G., 1982. Variations in the D/H and^{18}O/^{16}O ratios in cellulose extracted from a peat bog core. Earth and Planetary Science Letters 61, 283–290.

Cahill, A.T., Parlange, M.B., 1998. On water vapor transport in field soils. Water Resources Research 34, 731–739.
Carleton, T.J., Dunham, T.M.M., 2003. Distillation in a boreal mossy forest floor. Canadian Journal of Forest Research 33, 663–671.
Clymo, R.S., Hayward, P.M., 1982. The Ecology of *Sphagnum*. In: Smith, A.J.E. (Ed.), Bryophyte Ecology. Chapman and Hall, London, pp. 229–288.
Coleman, M.L., Shepherd, T.J., Durham, J.J., Rouse, J.E., Moore, G.R., 1982. Reduction of water with zinc for hydrogen isotope analysis. Analytical Chemistry 54, 993–995.
Collis-George, N., 1959. The physical environment of soil animals. Ecology 40, 550–557.
Coplen, T.B., 1996. New guidelines for reporting stable hydrogen, carbon, and oxygen isotope-ratio data. Geochimica et Cosmochimica Acta 60, 3359–3360.
Craig, H., Gordon, L.I., 1965. Deuterium and oxygen-18 variations in the ocean and marine atmosphere. In: Tongiorgi, E. (Ed.), Stable Isotopes in Oceanographic Studies and Paleotemperatures. Laboratorio di Geologia Nucleare, Pisa, Italy, pp. 9–130.
Cuntz, M., Ogée, J., Farquhar, G., Peylin, P., Cernusak, L.A., 2007. Modelling advection and diffusion of water isotopologues in leaves. Plant, Cell and Environment 30, 892–909.
DePaolo, D.J., Conrad, M.E., Maher, K., Gee, G.W., 2004. Evaporation effects on oxygen and hydrogen isotopes in deep vadose zone pore fluids at Hanford, Washington. Vadose Zone Journal 3, 220–232.
Drexler, J.Z., Bedford, B.L., Scognamiglio, R., Siegel, D.I., 1999. Fine-scale characteristics of groundwater flow in a peatland. Hydrological Processes 13, 1341–1359.
Drimmie, R.J., Heemskerk, R.A., 1993. Water ^{18}O by CO_2 equilibration. Technical Procedure 13.0, Rev. 02. Environmental Isotope Laboratory: Department of Earth Sciences, University of Waterloo. 11pp.
Edwards, T.W.D., 1993. Interpreting past climate from stable isotopes in continental organic matter. In: Swart, P.K., McKenzie, J., Lohmann, K.C., Savin, S. (Eds.), Climate Change in Continental Isotopic Records, Geophysical Monograph, vol. 78. American Geophysical Union, Washington, DC, pp. 333–341.
Epstein, S., Mayeda, T.K., 1953. Variations in the $^{18}O/^{16}O$ ratio in natural waters. Geochimica et Cosmichimica Acta 4, 213.
Farquhar, G.D., Cernusak, L.A., 2005. On the isotopic composition of leaf water in the non-steady state. Functional Plant Biology 32, 293–303.
Flanagan, L.B., Brooks, J.R., Varney, G.T., Ehleringer, J.R., 1997. Discrimination against $C^{18}O^{16}O$ during photosynthesis and the oxygen isotope ratio of respired CO_2 in boreal forest ecosystems. Global Biogeochemical Cycles 11, 83–98.
Gan, K.S., Wong, S.C., Yong, J.W.H., Farquhar, G.D., 2003. Evaluation of models of leaf water ^{18}O enrichment using measurements of spatial patterns of vein xylem, leaf water and dry matter in maize leaves. Plant, Cell and Environment 26, 1479–1495.
Gates, D.M., 1980. Biophysical Ecology. Springer-Verlag, New York, Heidelberg, Berlin.
Gonfiantini, R., 1986. Environmental isotopes in lake studies. In: Fritz, P., Fontes, J.C. (Eds.), Handbook of Environmental Isotope Geochemistry, vol. 2. Elsevier, New York, pp. 113–168.
Govardhan, K., Alex, Z.C., 2005. MEMS based humidity sensor. In: Proceedings of the International Conference on Smart Materials Structures and Systems. Institute for Smart Structures and Systems ISSS-2005/SE-04, July 28–30, Bangalore, India, pp. SE20–SE27.
Hayward, P.M., Clymo, R.S., 1982. Profiles of water-content and pore-size in *Sphagnum* and peat, and their relation to peat bog ecology. Royal Society of London Series B – Biological Sciences Conference Proceedings 215 (1200), 299–325.
Horita, J., Wesolowski, D., 1994. Liquid–vapour fractionation of oxygen and hydrogen isotopes of water from the freezing to the critical temperature. Geochimica et Cosmochimica Acta 58, 3425–3497.
Hsieh, J.C.C., Chadwick, O.A., Kelly, E.F., Savin, S.M., 1998. Oxygen isotopic composition of soil water: quantifying evaporation and transpiration. Geoderma 82, 269–293.
Ingram, H.A.P., 1983. Hydrology. In: Gore, A.J.P. (Ed.), Ecosystems of the World 4A, Mires: Swamp, Bog, Fen and Moor. Elsevier, Amsterdam, pp. 67–158.
Ishihara, Y., Shimojima, E., Harada, H., 1992. Water vapor transfer beneath bare soil where evaporation is influenced by a turbulent surface wind. Journal of Hydrology 131, 63–104.
Izbicki, J.A., Radyk, J., Michel, R.L., 2000. Water movement through a thick unsaturated zone underlying an intermittent stream in the western Mojave Desert, Southern California, USA. Journal of Hydrology 238, 194–217.
Kellner, E., 2002. Surface energy fluxes and control of evapotranspiration from a Swedish *Sphagnum* mire. Agricultural and Forest Meteorology 110, 101–123.
Kellner, E., Halldin, S., 2002. Water budget and surface-layer water storage in a *Sphagnum* bog in central Sweden. Hydrological Processes 16, 87–103.
Kellner, E., Waddington, J.M., Price, J.S., 2005. Dynamics of biogenic gas bubbles in peat: potential effects on water storage and peat deformation. Water Resources Research 41, W08417. doi:10.1029/2004WR003732.
Kennedy, P., Van Geel, P.J., 2000. Hydraulics of peat filters treating septic tank effluent. Transport in Porous Media 41, 47–60.
Kim, J., Verma, S.B., 1996. Surface exchange of water vapour between an open *Sphagnum* fen and the atmosphere. Boundary-Layer Meteorology 79, 243–264.
Klute, A. (Ed.), 1986. Methods of Soil Analysis Part 1 Physical and Mineralogical Methods, second ed. American Society of Agronomy, Madison, WI.
Mathieu, R., Bariac, T., 1996. A numerical model for the simulation of stable isotope profiles in drying soils. Journal of Geophysical Research D 101, 12685–12696.
McNeil, P., Waddington, J.M., 2003. Moisture controls on *Sphagnum* growth and CO_2 exchange on a cutover bog. Journal of Applied Ecology 40, 354–367.
Millington, R.J., 1959. Gas diffusion in porous media. Science 130, 100–102. doi:10.1126/science.130.3367.100-.
Millington, R., Quirk, J.P., 1961. Permeability of porous solids. Transactions of the Faraday Society 57, 1200.
Moldrup, P., Olesen, T., Schjonning, P., Yamaguchi, T., Rolston, D.E., 2000. Predicting the gas diffusion coefficient in undisturbed soil from soil water characteristics. Soil Science Society of America Journal 64, 94–100.
Monteith, J.L., 1965. Evaporation and the environment. In: Proceedings of the 19th Symposium of the Society of Experimental Biology, pp. 205–234.
Münnich, K.O., Sonntag, C., Christmann, D., Thoma, G., 1980. Isotope fractionation due to evaporation from sand dunes. ZFI – Mitteilungen, Zentralinstitut für Isotopen und Strahlenforschung 29, 319–322.
Nichols, D.S., Brown, J.M., 1980. Evaporation from a *Sphagnum* moss surface. Journal of Hydrology 48, 289–302.
Ogée, J., Cuntz, M., Peylin, P., Bariac, T., 2007. Non-steady-state, non-uniform transpiration rate and le af anatomy effects on the progressive stable isotope enrichment of le af water along monocot le aves. Plant, Cell and Environment 30, 367–387.
Price, J.S., 2003. Role and character of seasonal peat soil deformation on the hydrology of undisturbed and cutover peatlands. Water Resources Research 39 (9), 1241. doi:10.1029/2002WR001302,2003.
Price, J.S., 1991. Evaporation from a blanket bog in a foggy coastal environment. Boundary-Layer Meteorology 57, 391–406.
Reeve, A.S., Siegel, D.I., Glaser, P.H., 2000. Simulating vertical flow in large peatlands. Journal of Hydrology 227, 207–217.
Rose, C.W., 1968. Water transport in soil with a daily temperature wave I. Theory and experiment Australian Journal of Soil Research 6, 31–44.
Rydin, H., Clymo, R.S., 1989. Transport of carbon and phosphorus compounds about *Sphagnum*. Proceedings of the Royal Society of London B 237, 63–84.
Stern, L., Baisden, W.T., Amundson, R., 1999. Processes controlling the oxygen isotope ratio of soil CO_2: analytic and numerical modelling. Geochimica et Cosmochimica Acta 63, 799–814.
Tetens, O., 1930. Uber Einige Meterologische Begriffe. Zeitschrift für Geophysik 6, 297–309.
Touma, J., Vachaud, G., Parlange, J.Y., 1984. Air and water-flow in a sealed, ponded, vertical soil columns – experiment and model. Soil Science 137, 181–187.
University of Waterloo, 2006. University of Waterloo Weather Station <weather.uwaterloo.ca> (accessed 12.12.06).
Walker, G.R., Hughes, M.W., Allison, G.B., Barnes, C.J., 1988. The movement of isotopes of water during evaporation from a bare soil surface. Journal of Hydrology 97, 181–197.
Williams, T.G., Flanagan, L.B., 1996. Effect of changes in water content on photosynthesis, transpiration and discrimination against $^{13}CO_2$ and $C^{18}O^{16}O$ in *Pleurozium* and *Sphagnum*. Oecologia 108, 38–46.
Yazaki, T., Urano, S.I., Yabe, K., 2006. Water balance and water movement in unsaturated zones of *Sphagnum* hummocks in Fuhrengawa Mire, Hokkaido, Japan. Journal of Hydrology 319, 312–327.
Yoshikawa, K., Bolton, W.R., Romanovsky, V.E., Fukuda, M., Hinzman, L.D., 2002. Impacts of wildfire on the permafrost in the boreal forests of Interior Alaska. Journal of Geophysical Research 107, 8148. doi:10.1029/2001JD000438.
Zimmermann, U., Ehhalt, D., Münnich, K.O., 1967. Soil water movement and evapotranspiration: changes in the isotopic composition of the water. In: Isotopes in Hydrology. IAEA, Vienna, pp. 567–584.